NRC Research Press

ARTICLE

The critical state line of nonplastic tailings

L.A. Torres-Cruz and J.C. Santamarina

Abstract: The probability of failure of tailing dams and associated risks demand improvements in engineering practice. The critical state line provides a robust framework for the characterization of mine tailings. New experimental data for nonplastic platinum tailings and a large database for tailings and nonplastic soils (grain size between 2 and 500 μm) show that the critical state parameters for nonplastic tailings follow the same trends as nonplastic soils as a function of particle-scale characteristics and extreme void ratios. Critical state lines determined for extreme tailings gradations underestimate the range of critical state parameters that may be encountered in a tailings dam; in fact, mixtures with intermediate fines content exhibit the densest granular packing at critical state. The minimum void ratio e_{min} captures the underlying role of particle shape and grain size distribution on granular packing and emerges as a valuable index property to inform sampling strategies for the assessment of spatial variability. Mineralogy does not significantly affect the intercept Γ_{100}, but it does affect the slope λ. The friction coefficients M of tailings are similar to those of other nonplastic soils; while mineralogy does not have a significant effect on friction, more angular grains lead to higher friction coefficients.

Key words: tailings, critical state line, minimum void ratio, nonplastic soils.

Résumé : La probabilité de défaillance des digues à stériles et les risques associés exigent des améliorations dans la pratique de l'ingénierie. La ligne d'état critique fournit un cadre solide pour la caractérisation des résidus miniers. De nouvelles données expérimentales sur les résidus de platine non plastiques et une importante base de données sur les résidus et les sols non plastiques (granulométrie comprise entre 2 et 500 μm) montrent que les paramètres de l'état critique des résidus non plastiques suivent les mêmes tendances que les sols non plastiques en fonction des caractéristiques granulométriques et des taux extrêmes de vides. Les lignes d'état critique déterminées pour les gradations extrêmes des résidus sous-estiment l'éventail des paramètres d'état critique que l'on peut rencontrer dans une digue à résidus. En fait, les mélanges à teneur intermédiaire en fines présentent l'emballage granulaire le plus dense à l'état critique. Le taux minimal de vide e_{min} saisit le rôle sous-jacent de la forme des particules et de la distribution granulométrique sur l'emballage granulaire, et s'avère une propriété d'indice précieuse pour éclairer les stratégies d'échantillonnage pour l'évaluation de la variabilité spatiale. La minéralogie n'affecte pas significativement l'interception Γ_{100} mais elle affecte la pente λ. Les coefficients de frottement M des résidus sont semblables à ceux des autres sols non plastiques Bien que la minéralogie n'ait pas d'effet significatif sur le frottement, des grains plus angulaires entraînent des coefficients de frottement plus élevés. [Traduit par la Rédaction]

Mots-clés : résidus, limite d'état critique, taux de vides minimal, sols non plastiques.

Introduction

The historical failure rate of tailing dams and the associated risks demand improvements in material characterization, the design of the containment structure, construction practices, and monitoring technology (Santamarina et al. 2019). The critical state line (CSL) provides a robust frame of reference for the assessment of mine tailings (Carrera et al. 2011; Castro et al. 1982; Fourie and Papageorgiou 2001; Jefferies and Been 2015; Li et al. 2018; Vermeulen 2001). The CSL swings through the confinement–shear–volume space (p'–q–e) and generates two projections. The q–p' projection is the linear Coulomb strength model

$$q = Mp' \quad (1)$$

where the M factor captures the frictional strength. The e–p' projection (Fig. 1) follows a semi-logarithmic trend

$$e = \Gamma_{p^*} - \lambda \log_{10}(p'/p^*) \quad (2)$$

where e is the void ratio, λ is the slope, p^* is an arbitrary reference stress, and the intercept Γ_{p^*} is the void ratio when $p' = p^*$. This study adopts $p^* = 100$ kPa to anchor the linear approximation in eq. 2 around stress levels that are relevant to field conditions. Although the reference stress p^* does not affect the critical state line (CSL) in itself, it does affect the strength of the correlations between Γ_{p^*} and other parameters (Torres-Cruz 2019). This manuscript adopts the classical definitions of the mean effective stress $p' = (\sigma'_1 + \sigma'_2 + \sigma'_3)/3$ and deviator stress $q = \sigma'_1 - \sigma'_3$.

There is strong lateral and vertical variability in grain size distribution within tailings dams (Carrera et al. 2011; Fourie and Papageorgiou 2001; Li 2017). Therefore, the proper selection of tailings samples is crucial to critical state characterization. One approach is to test the extreme, coarsest and finest, gradations in the deposit (Jefferies and Been 2015). However, this approach may be misleading as illustrated by multiple critical state studies of sand–silt mixtures (Papadopoulou and Tika 2008; Rahman and Lo 2008; Thevanayagam et al. 2002; Yang et al. 2006; Zlatović and Ishihara 1995); the critical state line (CSL) shifts downwards (a

Received 10 January 2019. Accepted 2 December 2019.

L.A. Torres-Cruz. University of the Witwatersrand, Johannesburg, South Africa.
J.C. Santamarina. King Abdullah University of Science and Technology (KAUST), Thuwal, Saudi Arabia.
Corresponding author: L.A. Torres-Cruz (email: LuisAlberto.TorresCruz@wits.ac.za).

Fig. 1. Typical critical state line (CSL) and its idealization in e–$\log_{10}(p')$ space. The choice of Γ_{100} avoids extrapolation effects. [Colour online.]

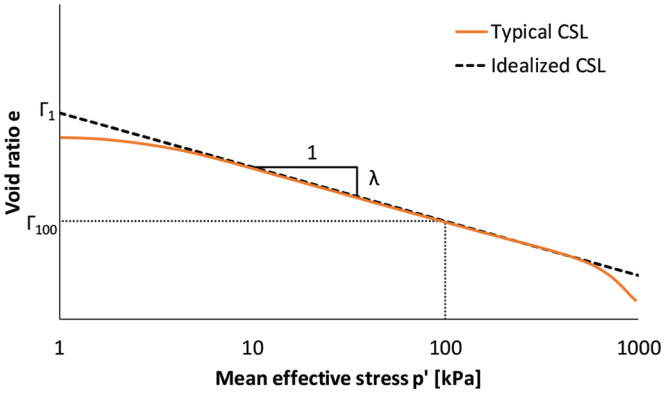

reduction in Γ_{p^*}) as the silt content increases from 0% to ~30%, but it shifts upwards (an increase in Γ_{p^*}) as the silt content exceeds 30%. Therefore, analyses based on the two extreme gradations underestimate the range of critical states present at a nonplastic tailings dam.

Previous studies report a correlation between the intercept Γ_{100} and the minimum void ratio e_{min} for nonplastic soils (Cho et al. 2006; Torres-Cruz 2019). In addition, there is some correlation (*i*) between the slope λ and the gap between extreme void ratios (e_{max}–e_{min}), i.e., the volumetric compression potential (Cho et al. 2006; Cubrinovski and Ishihara 2000), and (*ii*) between λ and e_{min}, i.e., e_{min} alone can provide some information on volumetric compressibility (Torres-Cruz 2019). Overall, these trends capture the underlying role of particle shape and grain size distribution on granular packing and extreme void ratios e_{max} and e_{min} (Cho et al. 2006; Torres-Cruz 2019). Traditionally, extreme void ratios are used to characterize coarse-grained soils, i.e., retained on sieve #200. However, they can be equally useful to characterize the behavior of nonplastic silts (Lade et al. 1998; Carrera et al. 2011; Park and Santamarina 2017; Li and Coop 2019; Torres-Cruz 2019).

The scatter in the trends between critical state parameters and extreme void ratios may be too high for reliable predictions of Γ_{100} and λ. However, these correlations suggest the possibility that an easily measured index property could assist in assessing the potential spatial variability of critical state parameters in nonplastic tailings, such as those that result from the extraction of gold, platinum, copper, and iron (Bedin et al. 2012; Li et al. 2018; Li 2017; Li and Coop 2019; this work — Note: kimberlite and some types of iron tailings can exhibit considerable plasticity).

This study explores the determination of the critical state line (CSL) of nonplastic platinum tailings, analyzes results in the context of a large database of CSLs compiled from the literature (25 nonplastic tailings and 132 nonplastic soils), and seeks to identify trends between critical state parameters (Γ_{100}, λ, and M) and index properties that can be used to readily assess spatial variability in tailings dams.

Triaxial testing program

Materials and methods: platinum tailings

Platinum tailings were sourced from the upper beach of an upstream spigotted tailings dam located in the North West Province of South Africa. The tailings are nonplastic, angular-shaped (Fig. 2), and have a complex mineralogy dominated by enstatite (27%), bytownite (27%), chromite (21%), and hornblende (8%), with traces (<5%) of diopside, epidote, talc, and biotite, among other minerals (Amponsah-Dacosta 2017).

The laboratory investigation centers around six mixtures prepared with pre-sieved tailings fractions. The mixtures have a fines content (FC) that ranges from 10% to 98% (Fig. 3 and Table 1 — Note: fines are <75 μm). This range of FC covers field observations (from 33% to 95%; Torres-Cruz 2016). This study follows two methods to measure e_{min}: the standard ASTM D1557 (ASTM 2002*a*) and a nonstandard method that benefits from a small sample size (similar to that proposed by Lade et al. 1998, as described in Torres-Cruz 2016). Although not applicable to FC > 15%, this study involved the ASTM D4254 (ASTM 2000) to measure e_{max} due to a lack of a standardized alternative. Figure 4 presents e_{max} and e_{min} values for the six mixtures and shows similar trends for e_{min} values gathered with the two methods. Clearly, the extreme specimens (FC = 10% and 98%) exhibit the highest e_{max} and e_{min}. Conversely, the lowest values correspond to mixtures with 30% ≤ FC ≤ 47%, in agreement with other studies of sand–silt mixtures (Papadopoulou and Tika 2008; Rahman and Lo 2008; Thevanayagam et al. 2002; Yang et al. 2006; Zlatović and Ishihara 1995; Park and Santamarina 2017).

Based on these results, critical state testing focused on three mixtures with distinctly different e_{min} values: FC = 10%, 30%, and 81%. The preparation of triaxial test specimens (70 mm diameter, 141 mm height) involved moist tamping to achieve loose contractive specimens (Ishihara 1993) to minimize strain localization (Jefferies and Been 2015 — Note: ends were not lubricated as nonuniform radial strains may remain; refer to Rees 2010). Air-CO_2 replacement prior to water injection and back-pressure produced high degrees of saturation; in fact, all specimens exhibited a Skempton's parameter $B \geq 0.96$. The stress path consisted of isotropic consolidation applied in a single stage followed by monotonic shearing, either under drained (CD) or undrained (CU) conditions. The displacement-controlled loading frame applied the deviatoric stress at constant cell pressure. Water content measurements at the end of the test enabled void ratio determinations (refer to Verdugo and Ishihara 1996). Table 2 presents a summary of the testing program (additional experimental details in Torres-Cruz 2016).

Results

Figure 5 illustrates typical response curves obtained for platinum tailings specimens subjected to drained and undrained loading in terms of deviatoric stress q, pore pressure u, and void ratio e vs. vertical strain ε_a. The hyperbolic model fitted to the pre-peak portion of the deviatoric stress vs. axial strain curve q–ε_a corrected early seating and misalignment effects and identified the true start of loading (Bishop and Henkel 1957).

On the other end of the response curves, most specimens do not reach stable pore pressure u (CU tests) or void ratio e (CD tests) within the strain level attainable in triaxial tests (Fig. 5). Several authors have suggested extrapolation procedures that allow for improved estimates of critical state conditions (Li 2017; Murthy et al. 2007). The following criteria were implemented in this study (Fig. 6 — refer to Carrera et al. 2011): (Fig. 6*a*) extrapolate q/p' to $\delta u/\delta\varepsilon_a = 0$ for undrained tests, (Fig. 6*b*) extrapolate q–p' trends to asymptotic M, and (Fig. 6*c*) extrapolate void ratio to the critical state condition of zero dilatancy $\delta\varepsilon_v/\delta\varepsilon_a = 0$ for drained tests. Table 2 summarizes the critical state values determined for all tests.

Figure 7 shows the critical states for all CD and CU tests for the three selected mixtures. The CSLs on the e–p' projection follow the semi-log linearization and are distinctly different for the three mixtures (Fig. 7*a*). More importantly, the intercept Γ_{100} is lowest for the mixture with fines content (FC) = 30%, in agreement with extreme void ratio trends (Fig. 4). Figure 7*b* shows the q–p' projections of the CSLs; the computed M values for the three mixtures fall within a narrow range of $M = 1.27 \pm 0.02$. This is consistent with previous results that show that M is largely independent of grain size distribution (Bandini and Coop 2011; Carrera et al. 2011; Li et al. 2015). Table 1 lists the values of Γ_{100}, λ, and M for each mixture. Distinctly different e–p' projections but indistinguishable q–p' projections imply that the dilative tendency of a speci-

Fig. 2. Scanning electron microscope images of platinum tailings: (*a*) coarse, (*b*) intermediate, and (*c*) fine particles.

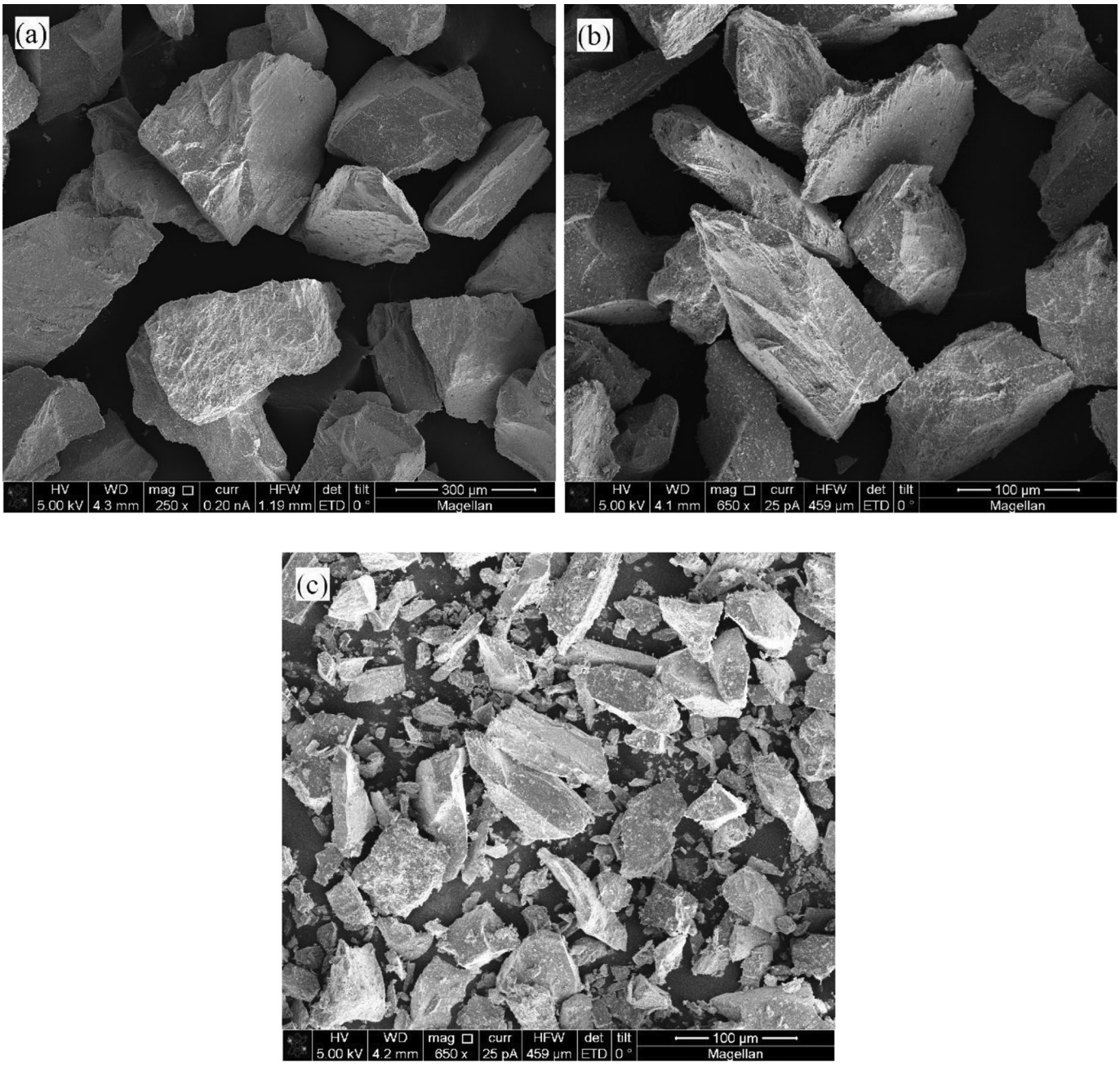

Fig. 3. Particle size distribution curves of platinum tailings.

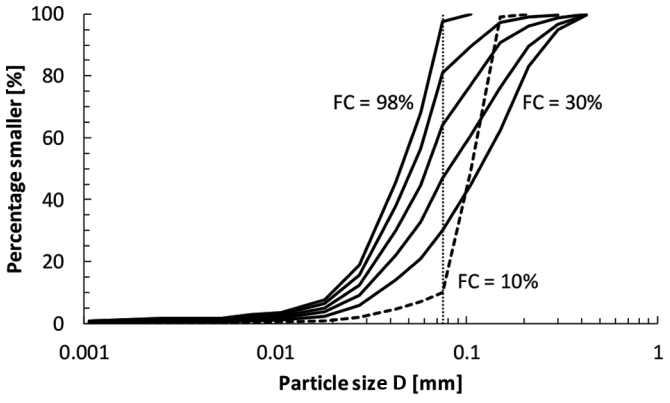

men at an initial e_o and p'_o will depend on its gradation; yet, gradation will not affect the stress ratio the specimen will reach at critical state.

Insights from the database

Data sources

The following analyses take into consideration the critical state lines (CSLs) of the three platinum mixtures described above, 25 tailings reported in the literature (Table 3), and 132 nonplastic soils collected from published studies (including natural soils and material from rock crushers; Torres-Cruz 2019). Figure 8 illustrates the range in particle size distributions — between 2 and 500 μm — for tailings in the database.

Uncertainty in Γ_{100} and λ

The least squares solution identifies model parameters by minimizing the sum of squared errors SSE = $\Sigma(e_m - e_p)^2$ between mea-

Table 1. Properties of mixtures of platinum tailings.

FC (%)	D_{50} (μm)	C_u[a]	G_s[b]	e_{min}[c]	e_{min}[d]	e_{max}[e]	Γ_{100}	λ	M
10	106	1.5	3.51	0.70	—	1.08	1.05	0.076	1.25
30	118	4.2	3.43	0.53	0.59	0.90	0.81	0.042	1.29
47	81	3.7	3.48	0.52	0.58	0.93	—	—	—
64	62	3.0	3.54	0.59	0.61	0.93	—	—	—
81	52	2.8	3.59	0.63	0.66	1.12	0.92	0.069	1.25
98	45	2.6	3.61	0.65	0.68	1.18	—	—	—

[a]Coefficient of uniformity (D_{60}/D_{10}).
[b]Specific gravity, ASTM D854 (ASTM 2002*b*).
[c]Nonstandard procedure.
[d]ASTM D1557 (ASTM 2002*a*).
[e]ASTM D4254 (ASTM 2000).

Table 2. Critical state values and end of test conditions of triaxial tests on platinum tailings.

			Critical state values				
FC (e_{min})	Test ID	Test type	e	p' (kPa)	q (kPa)	M	End of test condition[a]
Low 10% (0.70)	10-1	CU	1.020	177	216	1.22	Critical state
	10-2	CU	1.040	145	174	1.20	Critical state
	10-3[b]	CD	1.018	328	384	1.17	$\delta\varepsilon_v/\delta\varepsilon_a = -0.03$
	10-4	CU	1.040	105	131	1.25	$\delta u/\delta\varepsilon_a = -0.6$ kPa/%
	10-5	CD	0.992	469	612	1.30	Critical state
	10-6[b]	CU	1.056	95	117	1.23[c]	$\delta u/\delta\varepsilon_a = -2.5$ kPa/%
Medium 30% (0.53)	30-1	CU	0.755	540	701	1.30	Critical state
	30-2	CU	0.813	90	118	1.31	$\delta u/\delta\varepsilon_a = -0.2$ kPa/%
	30-3	CU	0.806	138	178	1.29	Critical state
	30-4	CU	0.812	144	187	1.29	$\delta u/\delta\varepsilon_a = 1$ kPa/%
	30-5	CU	0.808	77	101	1.30	$\delta u/\delta\varepsilon_a = 0.8$ kPa/%
	30-6[b]	CD	0.802	285	368	1.29[c]	$\delta\varepsilon_v/\delta\varepsilon_a = 0.02$
	30-7[b]	CD	0.773	502	648	1.29[c]	$\delta\varepsilon_v/\delta\varepsilon_a = 0.03$
High 81% (0.63)	81-1[b]	CU	0.885	326	408	1.25	$\delta u/\delta\varepsilon_a = -4$ kPa/%
	81-2[b]	CU	0.889	335	419	1.25[c]	$\delta u/\delta\varepsilon_a = -5.5$ kPa/%
	81-3[b]	CU	0.891	335	415	1.24	$\delta u/\delta\varepsilon_a = -5$ kPa/%
	81-4	CU	0.916	119	146	1.23	Critical state
	81-5	CD	0.879	448	568	1.27	$\delta\varepsilon_v/\delta\varepsilon_a = -0.03$
	81-6[b]	CU	0.914	175	215	1.23	$\delta u/\delta\varepsilon_a = -2.5$ kPa/%
	81-7	CD	0.892	239	303	1.27	$\delta\varepsilon_v/\delta\varepsilon_a = -0.01$

[a]Sign convention: positive for contraction and negative for dilation.
[b]Extrapolation scheme applied.
[c]Average M value of other tests done on the same mixture.

sured (e_m) and predicted (e_p) void ratios at critical state. Let's consider critical state data for six tailings and (*i*) identify the optimal Γ_{100} and λ values and then (*ii*) vary either Γ_{100} or λ to compute slices of the error surface across the optimum set (Santamarina and Fratta 2006). The horizontal axes in Fig. 9 cover the range of possible Γ_{100} or λ values for nonplastic soils, as inferred from the database. The rate of convergence towards the minimum square error limits the accurate computation of the intercept Γ_{100} and slope λ for a given error. That is, the rate of convergence is a measure of invertibility; thus, Figs. 9*a* and 9*b* show that the intercept Γ_{100} is better inverted than the slope λ.

Alternatively, standard errors SE_λ and $SE_{\Gamma_{100}}$ reflect the uncertainty in λ and Γ_{100} through

$$(3)\qquad SE_\lambda = \sqrt{\frac{\left[\sum (e_p - e_m)^2/(N-2)\right]}{\sum \left(\log_{10}\frac{p'_m}{p'_{avg}}\right)^2}}$$

and

$$(4)\qquad SE_{\Gamma_{100}} = SE_\lambda \sqrt{\frac{\sum \left(\log_{10}\frac{p'}{100}\right)^2_m}{N}}$$

Fig. 4. Extreme void ratios vs. fines content of platinum tailings.

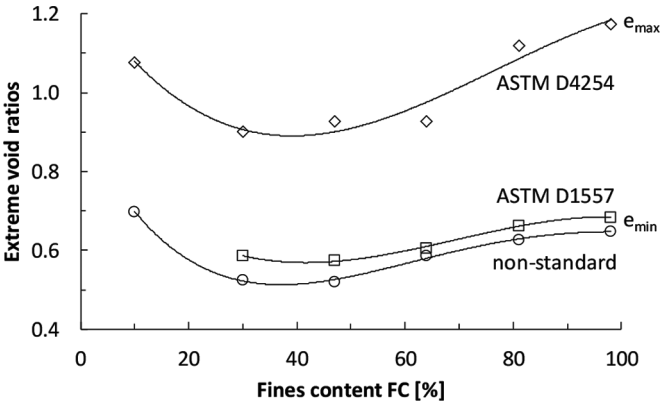

where N is the number of data points, and subindices stand for m = measured and avg = average (Navidi 2015). The normalizations $NSE_\lambda = SE_\lambda/\text{range}(\lambda)$ and $NSE_{\Gamma_{100}} = SE_{\Gamma_{100}}/\text{range}(\Gamma_{100})$ facilitate the analysis. Figure 10 compares the normalized standard errors $NSE_{\Gamma_{100}}$ and NSE_λ computed for 91 CSLs with known e–p' data points. The normalized error of the slope NSE_λ is 3 to 12 times

Fig. 5. Representative results of triaxial tests on platinum tailings: drained tests: (*a*) deviatoric stress q vs. axial strain ε_a, (*b*) void ratio e vs. ε_a; undrained tests: (*c*) q vs. ε_a, (*d*) pore pressure u vs. ε_a.

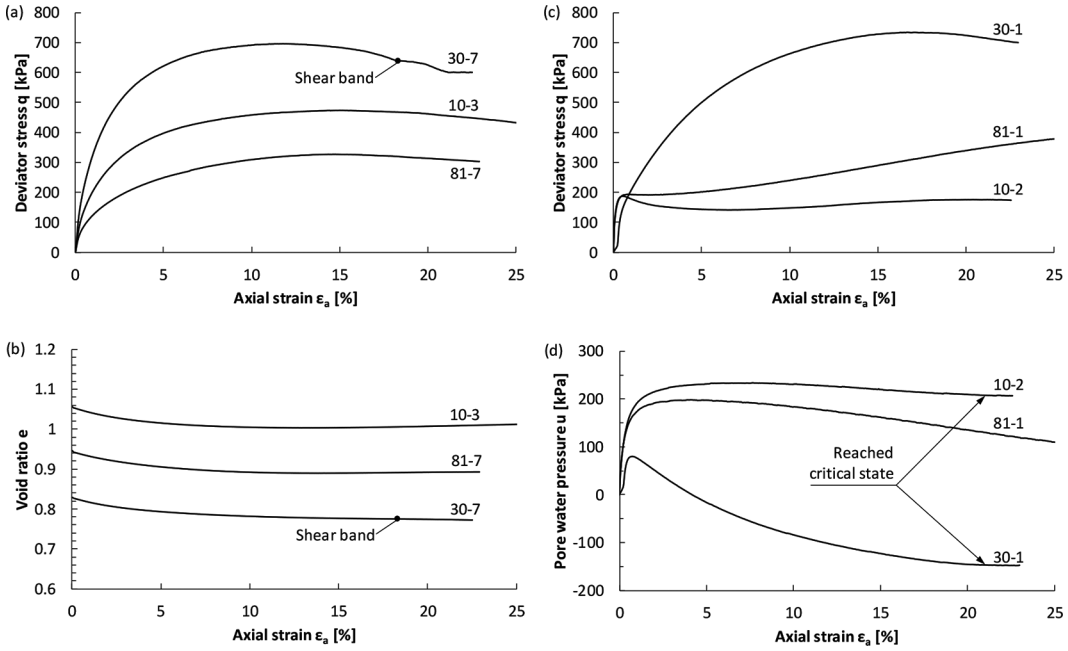

larger than the normalized error of the intercept $NSE_{\Gamma_{100}}$ in both tailings and nonplastic soils.

Critical state parameters and index properties

Previous studies showed that particle-scale characteristics such as shape and grain size distribution affect index properties and critical state parameters (Torres-Cruz 2019; Cho et al. 2006; Cubrinovski and Ishihara 2000). This section explores the correlation between index properties and critical state parameters for tailings and nonplastic soils. The database is dominated by soils that do not exhibit cementation or crushing at effective stress levels of interest, typically $\sigma' < 1$ MPa (see Jung et al. 2012 for the effect of cementation on critical state).

Figure 11 shows that tailings fall along the same Γ_{100}–e_{min} and Γ_{100}–e_{max} trends of other nonplastic soils. There is no clear clustering when the data are discriminated by mineralogy (not shown here). Furthermore, the intercept Γ_{100} is

- higher than the minimum void ratio for 96% of the database; the overall trend is $\Gamma_{100} \approx 1.4e_{min}$; thus, the spatial variability of e_{min} is a good indicator of potential spatial variability of Γ_{100} in nonplastic tailings
- lower than the maximum void ratio for 94% of the database; typically $\Gamma_{100} \approx 0.8e_{max}$.

Note that the spread in e_{max} is much higher than that in e_{min} ($1.2 \le e_{max}/e_{min} \le 2.2$, for 90% of the database). This hinders correlations that involve (e_{max}–e_{min}).

Figure 12*a* shows that tailings populate the same area as other nonplastic soils in the λ–e_{min} space. The range of possible slope values λ increases with e_{min}. In other words, the potential contractibility at critical state decreases for soils with low e_{min}; in fact $\lambda < (e_{min}/3)$ for 95% of the database. High hardness soils (e.g., quartz and silica) exhibit lower slopes (λ), mostly in the range of $\lambda < 0.10$ (Fig. 12*b*). Therefore, hardness affects contractiveness at critical state even though most of the data corresponds to intermediate stress levels where marked crushing is unlikely (all but one of the CSLs are defined for $p' < 4$ MPa). The scatter in Fig. 12 reflects the complex interactions among grain size distribution, particle shape, and mineralogy. The scatter also reflects the limited invertibility of the slope (refer to Figs. 9 and 10). There is no trend or clustering in plots of λ versus void ratio gap (e_{max}–e_{min}); however, note that the contraction in one log cycle λ is smaller than (e_{max}–e_{min}) for the entire database.

The relative contractiveness R_c shows the position of the CSL between two extreme density conditions (Verdugo and Ishihara 1996):

$$R_c = \frac{(e_{max})_{100} - \Gamma_{100}}{(e_{max})_{100} - (e_{min})_{100}} \quad (5)$$

where $(e_{max})_{100}$ and $(e_{min})_{100}$ are the void ratios attained by isotropically compressing the soil to 100 kPa from its loosest e_{max} and densest e_{min} conditions. The values of $(e_{max})_{100}$ and $(e_{min})_{100}$ are unknown for most soils; therefore, the estimate of R_c uses e_{max} and e_{min}. The computed relative contractiveness values for the database spreads the full $R_c = 0$ to 1 range (not shown here). Tailings cannot be distinguished from other nonplastic soils. There is a slight tendency for rounded soils to exhibit lower R_c than angular soils, and there is a weak inverse trend between R_c and median particle size D_{50}.

The database allows us to explore correlations with particle size. In particular:

- The maximum void ratio e_{max} is independent of particle size while $D_{50} > 100$ μm, but it increases for finer particles, probably due to electrostatic interactions (Fig. 13*a*).
- The minimum void ratio e_{min} and the intercept Γ_{100} are independent of particle size for all entries in the database (10 μm < D_{50} < 2000 μm; Figs. 13*b* and 13*c*); indeed, the effect of electrostatic interactions diminishes for the high energy conditions that prevail in e_{min} testing and under $p' = 100$ kPa (Santamarina 2003).

Figure 13*d* presents the friction parameter M vs. the median grain size D_{50}. The M value varies widely for tailings from $M = 1.1$ to 1.8, in a similar range to nonplastic soils. The associated variation in critical state friction angle is from $\varphi_{cs} = 27.7°$ to 43.8° (for reference, $M \approx 0.9$ or $\varphi_{cs} \approx 23°$ for glass beads). Previous studies have shown that mineralogy and particle angularity largely define the value of M (Cho et al. 2006; Sadrekarimi and Olson 2011; Li et al.

Fig. 6. Estimation of critical state parameters: extrapolation to critical state. Undrained test 81-1: (*a*) stress ratio q/p' vs. rate of pore pressure change $\delta u/\delta\varepsilon_a$ and (*b*) critical state in q–p'. Drained test 10-3: (*c*) void ratio e vs. dilatancy $\delta\varepsilon_v/\delta\varepsilon_a$.

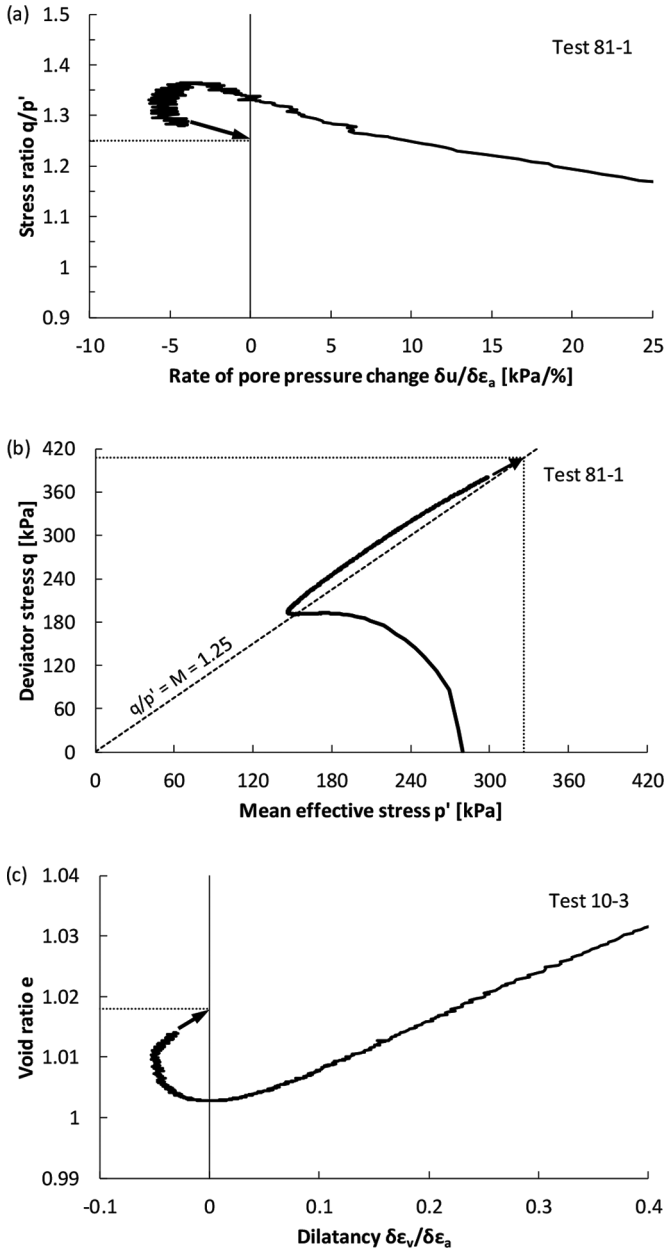

Fig. 7. Critical state lines for all mixtures of platinum tailings. (*a*) Projection on the void ratio vs. mean effective stress e–p' plane and (*b*) projection on the deviatoric vs. mean effective stress q–p' plane.

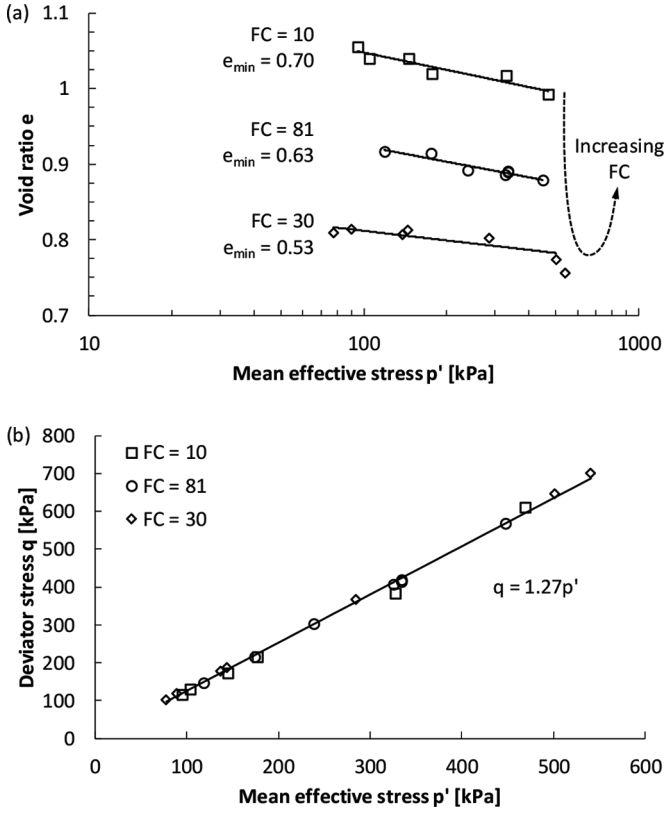

Fig. 8. Particle size distribution. Ranges for the tailings that are listed in Table 3 and reported in this work. Data are from references indicated in Table 3. Note: PLA refers to the platinum tailings reported herein. All other symbols are indicated in Table 3. The number next to each symbol indicates fines content. [Colour online.]

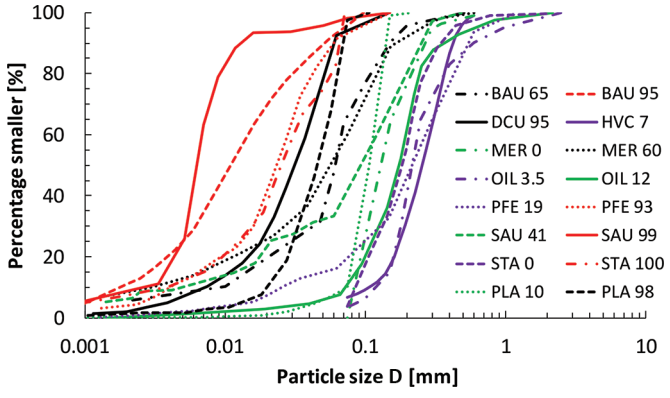

2015; Yang and Luo 2015). However, the database shows substantial overlap; the M value of angular soils is ~14% larger than that for rounded soils (Fig. 13*d*), and the data do not reveal any distinct effect of mineralogy on M.

Figures 11, 12, and 13 are based on published data produced by a large number of laboratories around the world. Therefore, there are potential differences in test protocols and data interpretation, including inconsistent assessment of particle shape and mineralogy. Then, apparent discrepancies between these results and previously reported observations from focused studies highlight the need for consistent assessment and reporting of soil properties.

Conclusions

This study explored critical state parameters for South African platinum tailings, identified critical state data for 25 other tailings, and considered additional data for 132 nonplastic soils previously reported in the literature. Inherent limitations in the strain levels attainable in triaxial tests hindered the determination of critical state; therefore, robust extrapolation strategies helped define consistent critical states for both drained and undrained tests.

The complete dataset allows the comparison of tailings with other nonplastic soils and the identification of trends between critical state parameters and index properties. Salient conclusions follow:

Fig. 9. Invertibility plots for (*a*) intercept Γ_{100} and (*b*) slope λ. Note: PLA refers to the platinum tailings reported herein. All other symbols are indicated in Table 3. The number next to each symbol indicates fines content. [Colour online.]

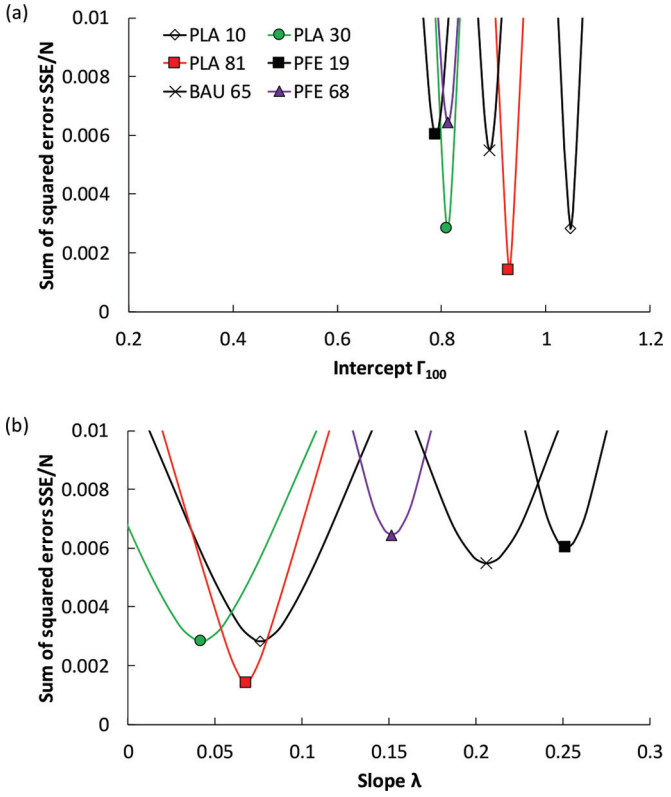

Fig. 10. Comparison between the normalized standard errors for the intercept $NSE_{\Gamma_{100}}$ and the slope NSE_{λ}. Note: PLA refers to the platinum tailings reported herein. All other symbols are indicated in Table 3. [Colour online.]

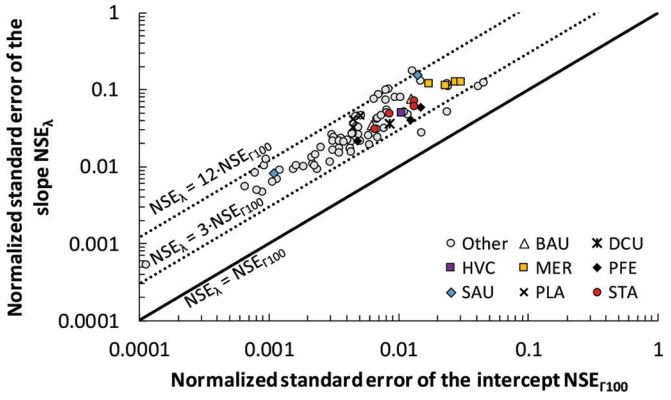

1. Data of void ratio vs. confinement e–p' at critical state extracted from triaxial test data allow the estimation of the intercept Γ_{100} at p' = 100 kPa with better accuracy than the estimation of the slope λ.
2. The critical state parameters for nonplastic tailings fall on the same trends as data for a wide range of nonplastic soils. This suggests that inferences about soil behavior made from nonplastic soils (nontailings) can be reasonably adopted for nonplastic tailings provided that these inferences account for potential differences in particle shape, grain size distribution, and mineralogy.

Fig. 11. Intercept Γ_{100} vs. (*a*) minimum void ratio e_{min} and (*b*) maximum void ratio e_{max}. Note: PLA refers to the platinum tailings reported herein. All other symbols are indicated in Table 3. [Colour online.]

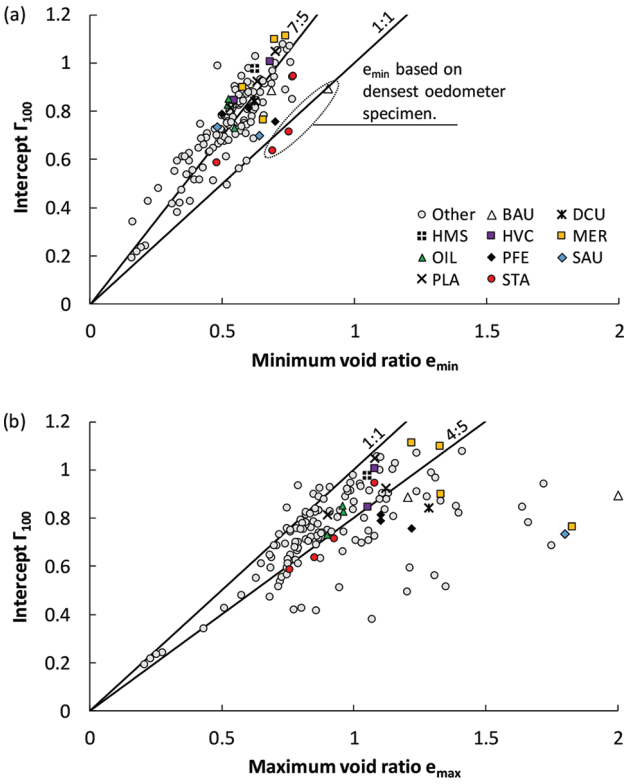

Fig. 12. Slope λ vs. minimum void ratio e_{min} with emphasis on (*a*) tailings and (*b*) mineralogy. Note: PLA refers to the platinum tailings reported herein. En/Byt/Chr refers to enstatite–bytownite–chromite, and Sil refers to silica. All other symbols are indicated in Table 3. [Colour online.]

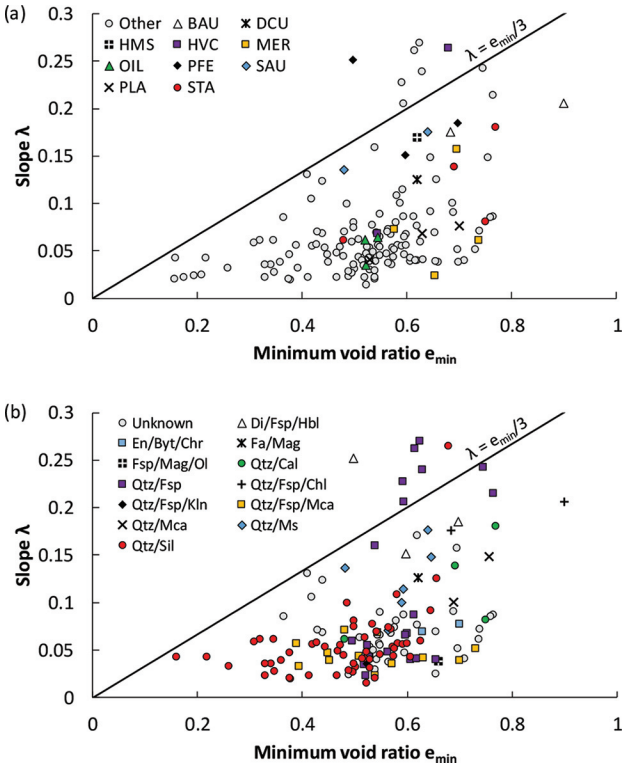

Table 3. Properties of tailings compiled from published studies.

Name (FC)	Symbol	D_{50} (μm)	C_u	e_{min}	e_{max}	Γ_{100}	λ	M	p' range (kPa)	G_s	Mineralogy[a]	Particle shape[b]	Reference
Brazilian Gold (65)	BAU	65	6.9	0.90	2.00	0.89	0.206	1.33	100–780	3.10	Qtz ≈ 27%, Ab ≈ 25%, Chl ≈ 35%	A-SA	Bedin et al. 2012;
Brazilian Gold (95)		10	7.7	0.68	1.20	0.89	0.176	1.41	30–900	2.89		A-SA	Li et al. 2018
Deixing Copper (95)	DCU	30	5.1	0.62	1.28	0.84	0.126	1.43	25–3700	3.75	Fa = 78%, Mag = 22%	A-SA	Li 2017
Hilton Mines (2.5)	HMS	200	—	0.62	1.05	0.98	0.17	1.42	50–1000	—	—	—	Jefferies and Been 2015
Lornex Copper (7)	HVC	260	2.7	0.68	1.08	1.00	0.264	1.40	70–1300	2.68	Qtz ≈ 100%	A	Castro et al. 1982
Highland Valley Copper (8)		200	2.8	0.54	1.06	0.84	0.068	—	1–220	2.66	Qtz = 36%, Mca = 27%, Ill = 15%, Fsp = 11%	A	Robertson et al. 2000; Wride et al. 2000
Merriespruit Gold (0)	MER	130	1.9	0.74	1.22	1.11	0.061	1.24	2–200	2.7	—	A-SA	Fourie and Papageorgiou
Merriespruit Gold (20)		120	4.7	0.70	1.33	1.10	0.157	1.17	7–80	2.7	—	A-SA	2001; Papageorgiou
Merriespruit Gold (30)		100	30	0.58	1.33	0.90	0.073	1.12	2–130	2.7	—	A-SA	2004; Tshabalala 2003
Merriespruit Gold (60)		60	25	0.66	1.83	0.76	0.024	1.19	10–125	2.7	—	A-SA	
Syncrude Oil Sand (3.5)	OIL	207	—	0.54	0.90	0.73	0.065	1.33	10–620	2.64	—	—	Jefferies and Been 2015
Syncrude Mildred Lake Oil Sand (10)		160	2.2	0.52	0.96	0.85	0.035	—	1–370	2.66	Qtz = 90%, Fsp = 5%, Kln = 5%	SA-SR	Robertson et al. 2000; Wride et al. 2000
Syncrude Oil Sand (12)		170	2.4	0.52	0.96	0.83	0.062	1.19	10–800	2.62	Qtz = 95%	A-SA	Sladen and Hanford 1987
Panzhihua Iron UB (19)	PFE	220	10	0.50	1.10	0.79	0.252	1.41	180–11 000	3.37	Di ≈ 35%, Lab ≈ 30%, Hbl ≈ 15%	A-SA	Li 2017; Li and Coop
Panzhihua Iron MB (68)		35	9.0	0.60	1.10	0.81	0.152	1.36	90–1900	3.14		A-SA	2019
Panzhihua Iron PO (93)		25	6.7	0.70	1.22	0.76	0.185	1.40	25–2000	3.11		A-SA	
Mizpah Dam Gold (72)	SAU	30	28	0.48	1.80	0.73	0.136	1.47	20–240	2.73	Qtz ≈ 75%, Ms ≈ 9%	A-SA	Vermeulen 2001
Pay Dam Gold (77)		25	22	0.64	2.10	0.70	0.176	1.40	30–200	2.74		A-SA	
Witwatersrand Gold UB (41)		90	23	—	1.24	—	—	1.56	50–600	2.72	Qtz ≈ 80%, traces of Ms, Prl, Ill	A-SA	Chang et al. 2011
Witwatersrand Gold MB (56)		50	11	—	1.65	—	—	1.78	40–210	2.69		A-SA	
Witwatersrand Gold PO (99)		5	3	—	3.00	—	—	1.62	130–330	2.75		A-SA	
Stava Fluorite (0)	STA	190	2.4	0.77	1.08	0.94	0.180	1.44	60–1100	2.72	Qtz ≈ 78%, Cal ≈ 10%	SA-SR	Carrera et al. 2011
Stava Fluorite (30)		130	9.7	0.69	0.85	0.63	0.138	1.45	45–1350	2.75		SA-SR	
Stava Fluorite (50)		75	10	0.48	0.76	0.58	0.061	1.44	15–770	2.78		SA-SR	
Stava Fluorite (100)		25	7.8	0.75	0.93	0.71	0.081	1.38	15–1220	2.83		SA-SR	

[a]Ab, albite; Cal, calcite; Chl, chlorite; Di, diopside; Fa, fayalite; Fsp, feldspar; Hbl, hornblende; Ill, illite; Kln, kaolinite; Lab, labradorite; Mag, magnetite; Mca, mica; Ms, muscovite; Prl, pyrophyllite; Qtz, quartz.
[b]A, angular; R, rounded; SA, subangular; SR, subrounded.

Fig. 13. Effect of median particle size D_{50} on (*a*) maximum void ratio e_{max}, (*b*) minimum void ratio e_{min}, (*c*) intercept Γ_{100}, and (*d*) friction ratio *M*. A & SA refers to angular and subangular; R & SR refers to rounded and subrounded. [Colour online.]

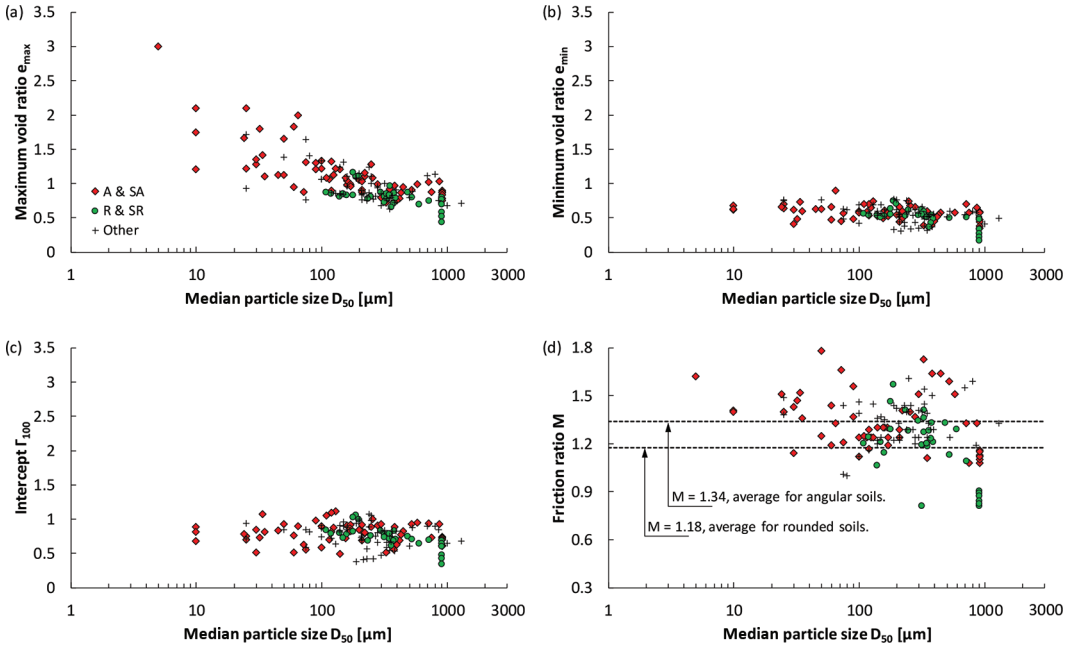

3. Mineralogy does not significantly affect the intercept Γ_{100} and related correlations, but it does affect the slope λ even when tests are conducted at intermediate stress levels below crushing. In fact, almost all high hardness soils (quartz and silica) have $\lambda < 0.10$, while soils with other mineralogies and variable hardnesses span the entire range of λ.
4. Published data and new experimental results show that the intercept Γ_{100} as well as the value of e_{min} are lowest for mixtures with intermediate fines content (FC), typically FC ≈ 30%. Therefore, the assessment of field conditions based on extreme gradations underestimates the range of critical state parameters in the tailings dam.
5. The spatial variability of e_{min} within a tailings deposit anticipates spatial variability in Γ_{100}. Additionally, the range of possible λ values increases with e_{min}. These observations can be used to inform sampling strategies.
6. The range of the friction coefficient *M* of tailings is similar to the range of values exhibited by other nonplastic soils. On average, angular soils exhibit greater *M* than rounded soils, in agreement with previous studies. Mineralogy and median particle size do not appear to significantly influence *M*.

Acknowledgements

This work was supported by the University of the Witwatersrand and King Abdullah University of Science and Technology (KAUST). G. Abelskamp edited the manuscript.

References

Amponsah-Dacosta, M. 2017. Mineralogical characterization of South African mine tailings with aim of evaluating their potential for the purposes of mineral carbonation [online]. M.Sc. thesis, Department of Geological Sciences, University of Cape Town, South Africa. Available from https://open.uct.ac.za/handle/11427/25014.

ASTM. 2000. D4254-00. Standard test methods for minimum index density and unit weight of soils and calculation of relative density. ASTM International, West Conshohocken, Pa., USA. doi:10.1520/D4254-00.

ASTM. 2002*a*. D1557-02. Standard test methods for laboratory compaction characteristics of soil using modified effort (56,000 lb-lbf/ft^3 (2,700 kN-m/m^3)). ASTM International, West Conshohocken, Pa., USA.

ASTM. 2002*b*. Standard test methods for specific gravity of soil solids by water pycnometer. ASTM standard D854. American Society for Testing and Materials, West Conshohocken, Pa., USA. doi:10.1520/D0854-02.

Bandini, V., and Coop, M.R. 2011. The influence of particle breakage on the location of the critical state line of sands. Soils and Foundations, **51**(4): 591–600. doi:10.3208/sandf.51.591.

Bedin, J., Schnaid, F., da Fonseca, A.V., and de Costa Filho, L.M. 2012. Gold tailings liquefaction under critical state soil mechanics. Géotechnique, **62**(3): 263–267. doi:10.1680/geot.10.P.037.

Bishop, A.W., and Henkel, D.J. 1957. The measurement of soil properties in the triaxial test. Edward Arnold (Publishers) Ltd., London.

Carrera, A., Coop, M., and Lancellotta, R. 2011. Influence of grading on the mechanical behaviour of Stava tailings. Géotechnique, **61**(11): 935–946. doi:10.1680/geot.9.P.009.

Castro, G., Enos, J., France, J.W., and Poulos, S. 1982. Liquefaction induced by cyclic loading. National Science Foundation, Washington, D.C.

Chang, N., Heymann, G., and Clayton, C. 2011. The effect of fabric on the behaviour of gold tailings. Géotechnique, **61**(3): 187–197. doi:10.1680/geot.9.P.066.

Cho, G.C., Dodds, J., and Santamarina, J.C. 2006. Particle shape effects on packing density, stiffness, and strength: natural and crushed sands. Journal of Geotechnical and Geoenvironmental Engineering, **132**(5): 591–602. doi:10.1061/(ASCE)1090-0241(2006)132:5(591).

Cubrinovski, M., and Ishihara, K. 2000. Flow potential of sandy soils with different grain compositions. Soils and Foundations, **40**(4): 103–119. doi:10.3208/sandf.40.4_103.

Fourie, A.B., and Papageorgiou, G. 2001. Defining an appropriate steady state line for Merriespruit gold tailings. Canadian Geotechnical Journal, **38**(4): 695–706. doi:10.1139/t00-111.

Ishihara, K. 1993. Liquefaction and flow failure during earthquakes. Géotechnique, **43**(3): 351–451. doi:10.1680/geot.1993.43.3.351.

Jefferies, M., and Been, K. 2015. Soil liquefaction: a critical state approach. CRC Press, Boca Raton, Fla., USA.

Jung, J.-W., Santamarina, J.C., and Soga, K. 2012. Stress-strain response of hydrate-bearing sands: Numerical study using discrete element method simulations. Journal of Geophysical Research, **117**: B04202. doi:10.1029/2011JB009040.

Lade, P., Liggio, C., and Yamamuro, J. 1998. Effects of non-plastic fines on minimum and maximum void ratios of sand. Geotechnical Testing Journal, **21**(4): 336–347. doi:10.1520/GTJ11373J.

Li, G., Liu, Y.-J., Dano, C., and Hicher, P.-Y. 2015. Grading-dependent behavior of granular materials: from discrete to continuous modeling. Journal of Engineering Mechanics, **141**(6): 04014172. doi:10.1061/(ASCE)EM.1943-7889.0000866.

Li, W. 2017. The mechanical behaviour of tailings [online]. Ph.D. thesis, Department of Architecture and Civil Engineering, City University of Hong Kong. Available from https://scholars.cityu.edu.hk/en/theses/the-mechanical-behaviour-of-tailings(d3d2338a-6cf2-4e19-993b-a3f67dad274a).html.

Li, W., and Coop, M.R. 2019. The mechanical behaviour of Panzhihua iron tailings. Canadian Geotechnical Journal, **56**(3): 420–435. doi:10.1139/cgj-2018-0032.

Li, W., Coop, M.R., Senetakis, K., and Schnaid, F. 2018. The mechanics of a silt-sized gold tailing. Engineering Geology, **241**: 97–108. doi:10.1016/j.enggeo.2018.05.014.

Murthy, T.G., Loukidis, D., Carraro, J.A.H., Prezzi, M., and Salgado, R. 2007. Undrained monotonic response of clean and silty sands. Géotechnique, **57**(3): 273–288. doi:10.1680/geot.2007.57.3.273.

Navidi, W. 2015. Statistics for engineers and scientists. McGraw Hill Education, New York.

Papadopoulou, A., and Tika, T. 2008. The effect of fines on critical state and liquefaction resistance characteristics of non-plastic silty sands. Soils and Foundations, **48**(5): 713–725. doi:10.3208/sandf.48.713.

Papageorgiou, G. 2004. Liquefaction assessment and flume modelling of the Merriespruit gold and Bafokeng platinum tailings [online]. Ph.D. thesis, Faculty of Engineering, University of the Witwatersrand, Johannesburg, South Africa. Available from http://wiredspace.wits.ac.za/handle/10539/23715.

Park, J.H., and Santamarina, J.C. 2017. Revised soil classification system for coarse–fine mixtures. Journal of Geotechnical and Geoenvironmental Engineering, **143**(8): 04017039.

Rahman, M.M., and Lo, S.R. 2008. The prediction of equivalent granular steady state line of loose sand with fines. Geomechanics and Geoengineering, **3**(3): 179–190. doi:10.1080/17486020802206867.

Rees, S.D. 2010. Effects of fines on the undrained behaviour of Christchurch sandy soils [online]. Ph.D. thesis, Department of Civil and Natural Resources Engineering, University of Canterbury, Christchurch, New Zealand. Available from https://ir.canterbury.ac.nz/handle/10092/3940.

Robertson, P.K., Wride, (Fear), C.E., List, B.R., Atukorala, U., Biggar, K.W., Byrne, P.M., et al. 2000. The CANLEX project: summary and conclusions. Canadian Geotechnical Journal, **37**(3): 563–591. doi:10.1139/t00-046.

Sadrekarimi, A., and Olson, S.M. 2011. Critical state friction angle of sands. Géotechnique, **61**(9): 771–783. doi:10.1680/geot.9.P.090.

Santamarina, J.C. 2003. Soil behavior at the microscale: particle forces. *In* Soil Behavior and Soft Ground Construction — The Ladd Symposium. ASCE Special Publications No. 119, MIT, Boston, Mass. pp. 25–56.

Santamarina, J.C., and Fratta, D. 2006. Concepts in discrete inverse problems. *In* Discrete signals and inverse problems: an introduction for engineers and scientists. John Wiley & Sons, Ltd., West Sussex, England. pp. 215–248. doi: 10.1002/0470021896.ch8.

Santamarina, J.C., Torres-Cruz, L.A., and Bachus, R.C. 2019. Why coal ash and tailings dam disasters occur. Science, **364**(6440): 526–528. doi:10.1126/science.aax1927.

Sladen, J.A., and Handford, G. 1987. A potential systematic error in laboratory testing of very loose sands. Canadian Geotechnical Journal, **24**(3): 462–466. doi:10.1139/t87-058.

Thevanayagam, S., Shenthan, T., Mohan, S., and Liang, J. 2002. Undrained fragility of clean sands, silty sands, and sandy silts. Journal of Geotechnical and Geoenvironmental Engineering, **128**(10): 849–859. doi:10.1061/(ASCE)1090-0241(2002)128:10(849).

Torres-Cruz, L.A. 2016. Use of the cone penetration test to assess the liquefaction potential of tailings storage facilities [online]. Ph.D. thesis, Faculty of Engineering and the Built Environment, University of the Witwatersrand, Johannesburg, South Africa. Available from http://wiredspace.wits.ac.za/handle/10539/22007.

Torres-Cruz, L.A. 2019. Limit void ratios and steady-state line of non-plastic soils. Proceedings of the Institution of Civil Engineers - Geotechnical Engineering, **172**(3): 283–295. doi:10.1680/jgeen.18.00011.

Tshabalala, L. 2003. The effect of consolidation and loading stress paths on the static liquefaction of mine tailings [online]. M.Sc. thesis, Faculty of Engineering and the Built Environment, University of the Witwatersrand, Johannesburg, South Africa. Available from http://wiredspace.wits.ac.za/handle/10539/23712.

Verdugo, R., and Ishihara, K. 1996. The steady state of sandy soils. Soils and Foundations, **36**(2): 81–91. doi:10.3208/sandf.36.2_81.

Vermeulen, N.J. 2001. The composition and state of gold tailings [online]. Ph.D. thesis, Faculty of Engineering, Built Environment and Information Technology, University of Pretoria, South Africa. Available from https://repository.up.ac.za/handle/2263/23079.

Wride, (Fear) C.E., Hofmann, B.A., Sego, D.C., Plewes, H.D., Konrad, J.-M., Biggar, K.W., et al. 2000. Ground sampling program at the CANLEX test sites. Canadian Geotechnical Journal, **37**(3): 530–542. doi:10.1139/t00-045.

Yang, J., and Luo, X.D. 2015. Exploring the relationship between critical state and particle shape for granular materials. Journal of the Mechanics and Physics of Solids, **84**: 196–213. doi:10.1016/j.jmps.2015.08.001.

Yang, S.L., Sandven, R., and Grande, L. 2006. Steady-state lines of sand–silt mixtures. Canadian Geotechnical Journal, **43**(11): 1213–1219. doi:10.1139/t06-069.

Zlatović, S., and Ishihara, K. 1995. On the influence of nonplastic fines on residual strength. *In* Proceedings of the 1st International Conference on Earthquake Geotechnical Engineering, Tokyo, Japan. AA Balkema, Rotterdam, the Netherlands. pp. 239–244.

List of symbols

CD	consolidated drained
CSL	critical state line
CU	consolidated undrained
D_{50}	median particle size
e	void ratio
e_m	measured void ratio
e_{max}	maximum void ratio
e_{min}	minimum void ratio
$(e_{max})_{100}$	void ratio attained after isotropic consolidation to 100 kPa from e_{max}
$(e_{min})_{100}$	void ratio attained after isotropic consolidation to 100 kPa from e_{min}
e_p	predicted void ratio
FC	fines content (percentage passing 75 μm sieve)
M	critical state friction ratio
N	number of data points
$NSE_{\Gamma_{100}}$	normalized standard error of the intercept Γ_{100}
NSE_λ	normalized standard error of the slope λ
p^*	arbitrary reference stress used to model the CSL in e–$\log_{10}(p'/p^*)$ space
p'	mean effective stress
p'_{avg}	average mean effective stress
p'_m	measured mean effective stress
q	deviator stress
R_c	relative contractiveness
$SE_{\Gamma_{100}}$	standard error of the intercept Γ_{100}
SE_λ	standard error of the slope λ
SSE	sum of squared errors
u	pore water pressure
Γ_{p^*}	critical state void ratio at a mean effective stress of p^*
ε_a	axial strain
ε_v	volumetric strain
λ	idealized slope of the CSL in e–$\log_{10}(p'/p^*)$ space
σ'_i	effective principal stress in the i direction
φ_{cs}	critical state friction angle